

Copyright © [2006] IEEE. Reprinted from

(Special Issue on Nonlocal, Collisionless Electron Transport in Plasmas - June 2006) .

This material is posted here with permission of the IEEE. Internal or personal use of this material is permitted. However, permission to reprint/republish this material for advertising or promotional purposes or for creating new collective works for resale or redistribution must be obtained from the IEEE by writing to pubs-permissions@ieee.org.

By choosing to view this document, you agree to all provisions of the copyright laws protecting it.

Non-Equilibrium EEDF in Gas Discharge Plasmas

Valery Godyak, Fellow of IEEE

Osram Sylvania, Beverly, MA 01915
valery.godyak@sylvania.com

Non-equilibrium effects associated with spatial and temporal nonlocality between electron energy distribution and electromagnetic field in gas discharge plasmas at low gas pressures are reviewed in this paper. Formation of non-equilibrium EEDF is discussed for capacitive and inductive rf discharges. The possibility of electron temperature control is considered for gas discharge plasmas at non-equilibrium condition.

1. Introduction

Partially ionized gas discharge plasmas at low gas pressures are always in a non-equilibrium state. In particular, in such plasmas, electrons are not in a thermal equilibrium with neutral species and ions. Indeed, the electron temperature, T_e , is much larger than the temperature of ions, T_i , and of neutrals T_g , ($T_e \gg T_i \geq T_g$). In addition, electrons are also not in equilibrium within their own ensemble, which results in a significant departure of the electron energy distribution function (EEDF), $F(\epsilon)$ from the equilibrium Maxwellian distribution. The main reason for this is the absence of a thermodynamic equilibrium between direct and reverse processes. For example, electron-ion creation and gas excitation are due to the impact of fast electrons in the plasma volume, while electron and radiation loss are due to plasma and radiation escape to the wall. Although, in general, Coulomb electron-electron collisions tend to support a Maxwellian EEDF, in gas discharge plasmas, the collision rate is usually too small, in order to bring the bulk of low energy electrons to an equilibrium with the high energy electrons responsible for inelastic collisions. Gas discharge plasmas are frequently called non-equilibrium, non-isothermal plasmas.

In this paper, we consider a different kind of non-equilibrium, namely, the spatial and/or temporal non-equilibrium between the electric field, E that sustains gas discharge plasma and the electron energy distribution, $F(\epsilon)$ that defines the plasma parameters and the rates of plasma-chemical processes, (E/F-non-equilibrium). An example of an extreme spatial non-equilibrium state is the plasma created by an electron beam, where electron acceleration takes place in an electron gun outside the plasma. A well known example of a temporal non-equilibrium state is the absence of rf oscillations in plasma parameters of rf discharges when the driving frequency is much larger than frequency of the electron energy loss.

In the last decades, low pressure rf discharges found wide applications in many branches of modern technology. A better understanding of rf discharges revealed the fundamental role of non-local and non-equilibrium

processes created by the electron thermal motion in a non-uniform plasma with a non-uniform electromagnetic field. Non-local electron kinetic effects [1-11], non-local electrodynamics [12-24] (like collisionless power absorption) and nonlinear phenomena at the plasma boundary in the rf sheath [2, 3, 25-28] and in the skin layer [29-35] are typical for low pressure rf discharges.

This paper is organized as follows. Basic processes in gas discharge plasmas when EEDF and thus other plasma parameters are in equilibrium with the electromagnetic field are analyzed in section 2 of the paper. Specifics of EEDF in the case of a non-uniform field and spatial non-locality are considered in section 3. Formation of non-equilibrium EEDF in low pressure capacitively coupled plasmas (CCP) and inductively coupled plasma (ICP) are considered in sections 4 and 5, respectively. Examples of EEDF control under conditions of temporal and spatial non-equilibrium are given in section 6. The paper ends with summarizing conclusions in section 7.

2. Plasma equilibrium in uniform heating field

Consider the classic approach to steady-state gas discharge plasmas. For given discharge geometry, kind of gas with pressure p , and power delivered to plasma electrons (i.e., discharge power P_d), the basic plasma parameters (the electron temperature T_e and the plasma density n) are determined by the ionization and electron energy balance. The ionization balance, governed by the continuity and momentum equations for the neutral plasma ($n_e = n_i = n$) with the Bohm criterion as the plasma boundary condition, yields the plasma spatial distribution $n(\mathbf{r})$ and the ionization frequency z as an eigenvalue of the problem.

In the approximation of the Maxwellian electron energy distribution function (EEDF), $F(\epsilon)$, and in the absence of nonlinear (with respect to the plasma density) processes of particle gain and loss (like stepwise ionization, attachment and volume recombination), the ionization frequency z_t found from the transport equations is a function of T_e , p and Λ , $z_t = z_t(T_e, p, \Lambda)$, and is independent of the discharge power and the plasma density. Here, p is the gas pressure and Λ is the characteristic size of the bounded plasma. This specific value of z_t provides the equilibrium between the volume plasma production and plasma loss to the wall, $z_t \langle n \rangle V = v_s \langle n_1 \rangle S$, where $\langle n \rangle$ is the volume averaged plasma density, $\langle n_1 \rangle$ is the surface averaged plasma density at the plasma boundary, V is the plasma volume, S the boundary surface ($V/S \approx \Lambda$), and $v_s = (T_e/M)^{1/2}$ is the ion sound speed.

On the other hand, ionization in the plasma volume is provided by collisions of fast electrons with molecules. The corresponding ionization frequency of this kinetic process is $z_k = N[v_e \sigma_i]$, and is therefore a function of the electron temperature and gas pressure, $z_k = z_k(T_e, p)$. Here, $N = p/T_g$ is the gas density, v_e is the electron velocity, σ_i is the ionization cross section, and $[]$ denotes averaging over the EEDF. Equating $z_t(T_e, p, \Lambda)$ and $z_k(T_e, p)$, we find for Maxwellian EEDF:

$$\langle n_1 \rangle v_s / \langle n \rangle \Lambda = z_t = z_k = CpT_e^{1/2}(1+2T_e/\epsilon_i)\exp(-\epsilon_i/T_e),$$

where $\langle n_1 \rangle / \langle n \rangle$ is a function of $p\Lambda$, and C is a constant that depends on the particular gas [36]. Thus, in bounded gas discharge plasmas with a given kind of gas, the electron temperature is a function of the product $p\Lambda$ and does not depend on the discharge power or the plasma density. Moreover, the electron temperature does not depend on the particular method of electron heating (T_e is determined only by the ionization balance). Hence, $T_e = T_e(p\Lambda)$ for all kinds of discharges, i.e., for dc, rf or microwave plasmas.

The electron energy balance for gas discharge plasmas provides equilibrium between the discharge power P_d , delivered from an external power source to the plasma electrons, and the electron loss power Q_e , associated with

electron-atom collisions and the escape of charged particles to the wall. In general, the energy balance equation has the form: $P_d = Q_e = 3/2 \cdot T_e \xi \langle n \rangle V$, where $\xi = Q_e^{-1} dQ_e/dt$ is the frequency of the electron energy loss. Accounting for all electron energy loss mechanisms, we obtain [37]:

$$\xi = 2\nu m/M + \Sigma 2\nu^* \varepsilon^*/3T_e + z \{ 2\varepsilon_i/3T_e + (4/3) + 1/3 [1 + \ln(M/2\pi m)] \}.$$

Here m is the electron mass and M is the ion mass, ν the electron-atom collision frequency and ν^* is the excitation collision frequency, ε^* the excitation energy and ε_i is the ionization energy. The first term on the right-hand side accounts for the electron elastic loss (gas heating); the second term accounts for atom excitations; and the last term accounts for wall losses, including ionization loss, electron escape to the wall and ion acceleration in the plasma ambipolar field and in the wall sheath. In fact, the electron thermal energy creates an ambipolar potential and an ion acceleration voltage across the wall sheath. Note that ξ depends on the electron temperature and is therefore a function of $p\Lambda$, independent of the discharge power and plasma density.

It should be noted that in some types of discharges, a significant (and in some case, the major) part of power from an external power source goes directly to ion acceleration. Examples of such discharges are: low pressure and high voltage CCPs where the main rf power absorption is associated with ion acceleration in rf sheaths (outside the plasma) [38,39], and Hall thrusters where ions are accelerated by dc electric field across magnetic field that suppress electron conductivity [40,41]. For such discharges the discharge energy balance should account for both, electron and direct ion heating.

A remarkable consequence of the electron energy balance in self sustained gas discharge plasmas is that the total number of plasma electrons (ions) N_p satisfies the relationship: $N_p = \langle n \rangle V = 2P_d/3\xi T_e$. Hence, for a fixed plasma volume V , the plasma density n is determined only by the discharge power and by the product $p\Lambda$, and is independent of the specific electron heating mechanism. Thus, the type of the low pressure discharge (dc, rf, mw) has no effect on the electron temperature and the plasma density for a given gas pressure, discharge geometry and power transferred to plasma electrons. This result is supported by experimental data [42] where similar processing rates were found for different kind of discharges.

When a uniform plasma along the heating electric field ($\nabla n \cdot \mathbf{E} = 0$) is maintained by a uniform electric field with an rms value E , and can be described adequately by the plasma conductivity $\sigma_p = e^2 n/m(\nu_{\text{eff}} + j\omega)$, the discharge power is $P_d = V \text{Re}[E^2 \langle \sigma_p \rangle]$. Equating P_d and Q_e one obtains:

$$E^2 = 3T_e m \xi \nu_{\text{eff}} (1 + \omega^2/\nu_{\text{eff}}^2)/2e^2,$$

where E is a function of $p\Lambda$ and ω/ν_{eff} and is independent of the discharge power and plasma density. Note that the effective electron collision frequency ν_{eff} may account for both collisional and collisionless heating processes [14, 36], and the collisional part of ν_{eff} can be essentially different for dc and rf fields [43]. Since in steady state plasmas the plasma density is proportional to the discharge power, the electric field E , as well as the electron temperature T_e are frozen at some equilibrium level that provide the ionization and electron energy balance. The plasma electric field is not affected by a slow increase in the discharge power if the plasma parameters remain in equilibrium with the rising power ($P_d^{-1} dP_d/dt \ll z$). In real plasmas, due to nonlinear processes (such as stepwise ionization and EEDF dependence on the plasma density) the electric field slightly drops with the discharge current. This is a well known effect of negative V/A characteristics of gas discharge plasmas.

The considerations above for uniform electric fields and uniform electron temperatures are also true for low pressure discharges with non Maxwellian EEDF as well as in the presence of nonlinear particle gain/loss effects (that usually play a secondary role). In this case, the EEDF and its scalar integrals (plasma density, effective electron temperature $T_{\text{eff}} = \frac{1}{2}m[v_e^2]$ and rates of elastic and inelastic collisions) are in equilibrium with the plasma sustaining electric field. The equilibrium EEDF is a result of the interplay between the electron energy gain in the electric field and the energy loss due to electron collisions with atoms, wall losses and electron energy redistribution caused by electron-electron collisions. Usually the EEDF is essentially different in elastic ($\epsilon < \epsilon^*$) and inelastic ($\epsilon > \epsilon^*$) electron energy ranges (ϵ^* is the excitation energy). For $\epsilon < \epsilon^*$, the EEDF is mainly governed by the function $v(\epsilon)$, the ratio ω/v , and by the electron-electron collision frequency ν_{ee} . For $\epsilon > \epsilon^*$, the EEDF is mainly governed by the electron inelastic collisions (excitation and ionization) and by the electron escape to the wall.

3. Plasma in non-uniform heating field

For low pressure dc and rf discharges in laboratory and in industrial applications, the plasma frequency $\omega_p = (4\pi e^2 n/m)^{1/2}$ is always much greater than the frequency ω of an externally applied plasma sustaining electromagnetic field ($\omega_p \gg \omega$). Under such conditions, the electromagnetic field is usually localized in a narrow boundary layer of width δ (skin depth in ICP, rf sheath width in CCP and cathode fall in dc glow discharge, GD), and the bounded non-uniform discharge plasma is sustained by a non-uniform heating field. The main electron heating process usually occurs in the boundary layer that constitutes just a small fraction of the whole discharge volume, $\delta < \Lambda$. The heating electromagnetic field can also be localized in a small area in the plasma bulk, when an external electromagnetic wave propagates deep into magnetized helicon and ECR plasmas [44, 45].

In bounded non-uniform plasmas, the lifetime of an average electron is too short to reach thermal equilibrium with atoms and ions. For that reason, in low pressure gas discharges, the electron temperature is much larger than the gas and ion temperatures. During its lifetime, an averaged electron bounces many times between discharge chamber walls in the potential well formed by the ambipolar potential $\phi < 0$ and the wall sheaths. At sufficiently low gas pressures (for argon roughly at $p\Lambda < 1$ Torr-cm), when the electron energy relaxation length $\lambda_\epsilon \approx \lambda(v/\xi)^{1/2}$ (where $\lambda \approx v_e v^{-1}$ is the electron free path with respect to the momentum transfer) is much larger than the plasma size ($\lambda_\epsilon \gg \Lambda$), an electron collides with atoms and crosses the plasma practically without changes in its total energy $\epsilon = \frac{1}{2}mv_e^2 + e\phi \approx \text{const}$. Under such conditions, which correspond to the limit of non-local electron kinetics [5-7], the electron energy distribution as a function of the electron total energy, $F(\epsilon)$, is almost uniform, i.e., $\nabla F(\epsilon) \approx 0$ over the electron accessible area ($\epsilon > 0$), and the plasma parameters T_e , n , v , v^* and v_i are non-local functions of the non-uniform heating electric field. Plasma electrons behave like a gas with infinite thermo-conductivity, and plasma parameter distributions are practically not correlated with the heating electromagnetic field distribution. In this case the mean electron kinetic energy $\langle \epsilon_k \rangle = \langle \frac{1}{2}mv_e^2 \rangle$ and the effective electron temperature $T_{\text{eff}} = \frac{2}{3}\langle \epsilon_k \rangle$ are not in equilibrium with the local electric field. The electron total energy and other plasma parameters, however, are in integral equilibrium with some spatially averaged electromagnetic field. On the other hand, for the local limit, when $\lambda_\epsilon \ll \Lambda$, the electron energy distribution $F(\epsilon)$, the electron temperature as well as the rates of electron collisions are local functions of the electric field. This case yields the local equilibrium between plasma parameters and the electric field, considered in the previous section.

Examples of non-locality features are given in Figs. 1 and 2 where plasma parameters and electron energy distributions were measured at different axial positions in a low pressure cylindrical ICP driven with flat spiral antenna at 6.78 MHz [22]. As can be seen in Fig.1, axial distributions of the electron temperature, plasma density and of the negative plasma potential are quite symmetrical with respect to the plasma midplane, in spite of the rf heating localized within a narrow skin layer ($\delta/2 \approx 1$ cm) on the coil side of the chamber (left in Fig. 1). In Fig. 2, the electron energy distribution, expressed in the terms of the electron energy probability function EEPF, $f(\epsilon) \sim \epsilon^{-1/2}F(\epsilon)$ that is measured at different distances from the quartz window (separating the plasma and rf coil), demonstrates the basic feature of non-local electron kinetics: the values of $f(\epsilon = \frac{1}{2}mv_e^2 + e\phi)$ measured at different positions in a non-uniform plasma with a non-uniform heating electric field are practically the same.

In practice, usually neither of the limiting cases occurs. In fact, in low pressure gas discharge plasmas ($p\Lambda < 1$ Torr-cm), although the electron kinetics are typically non-local, they do not correspond to any of the limiting cases. Due to a large disparity in values of λ_e for slow and fast electrons, the electrons in the elastic energy range ($\epsilon < \epsilon^*$), which account for the overwhelming majority of the electron population, exhibit mainly a non-local behavior:

$$\lambda_{\epsilon < \epsilon^*} \approx \lambda(2m/M + v_{ee}/v)^{-1/2} \gg \Lambda,$$

while the electrons in the inelastic energy range ($\epsilon > \epsilon^*$) behave nearly locally:

$$\lambda_{\epsilon > \epsilon^*} \approx \lambda(v/\xi)^{1/2} \leq \Lambda.$$

In this typical situation of plasma processing applications, the plasma uniformity control can be attained with a proper localization of the rf field, enhancing locally the high energy electron group that is responsible for the ionization process, while leaving the overwhelming low energy electron group to obey non-local kinetics.

A well-known example of strongly non-equilibrium conditions is the negative glow (NG) of a dc glow discharge. In a NG, plasma is produced by a swarm of high energy electrons, generated in the high voltage cathode sheath. The mean energy of those electrons is much larger than the electron energy in the positive column (PC), where the electron temperature is in equilibrium with the electric field. Therefore, the ionizing ability of these high energy electrons is much larger than that in the PC. The intense ionization in NG results in a self-organized structure where the plasma density is much larger than that in the PC, and the electron temperature and electric field are much smaller than those in the PC [46-49].

The EEDF of a NG differs significantly from the equilibrium EEDF observed in the positive column; it consists of a very small fraction of high energy electrons generated in the cathode sheath, and of the main body of cold electrons with their temperature close to the room temperature [46]. These cold electrons are not able to overcome the potential barrier of the cathode sheath where the electron heating occurs and they cannot be heated by the weak field in the NG. Thus, injection of hot electrons into the NG results in cooling of the main body of electrons.

Such a paradoxical, but rather universal feature of weakly ionized gas discharge plasmas, occurs “naturally” in different kinds of low pressure dc and rf discharges and manifests itself by an EEDF having a two-temperature structure in the elastic energy range. Examples of such phenomenon are a low energy peak in EEDF in the negative glow, in capacitive rf discharges, both in the α [1, 50] and in the γ [51, 52] modes, and in inductive rf discharges in the regime of anomalous skin effects [53, 54]. In all those cases, the EEDF is not in the local equilibrium with the heating electric field.

4. Non-equilibrium EEDF in CCP

Let us consider in more detail the formation of non-equilibrium EEDF for capacitive coupled plasma (CCP). Fig. 3 shows the evolution of EEPF $\sim \varepsilon^{-1/2}F(\varepsilon)$ with argon pressure, measured in the midplane of a 2 cm gap capacitively coupled discharge, driven at 13.56 MHz [1]. For relatively large argon pressures, in the collision-dominated regime ($\lambda < \Lambda$, $v^2 \gg \omega^2$), collisional rf power absorption takes place over the plasma volume, with EEDF and corresponding plasma parameters close to the equilibrium with rf electric field. In this case, the EEPF is Druyvesteyn-like, which is typical for Ramsauer gases at $v^2 \gg \omega^2$ in the absence of “Maxwellizing” e-e collisions. With a reduction in argon pressure or/and an increase in discharge current, electron heating localizes at the plasma boundary, and the convex EEPF becomes concave and can be represented as a bi-Maxwellian distribution. In this case, the discharge transits into the sheath heating mode. Depending on gas pressures, the heating mechanism in rf sheaths may be different: stochastic (collisionless) heating at low gas pressures and resistive (collisional) heating at elevated pressures. Fig. 4 shows the EEDF in the sheath heating mode (in a linear scale) and the corresponding EEPF (in a semi-log scale) for argon pressure 100 mTorr. Observe that the majority of electrons reside in the low energy group with $T_{e1} = 0.34$ eV and $n_1 = 1.32 \cdot 10^{10}$ cm⁻³, while $T_{e2} = 3.1$ eV and $n_2 = 1.3 \cdot 10^9$ cm⁻³ for the minority group.

The electron cooling mechanisms, associated with formation of the low energy peak of EEDF, in a CCP and a NG of dc glow discharge are similar and can be explained as follows [1,6,55]. In the sheath heating mode, the main electron heating is localized within the rf electrode sheaths having strong rf and dc electric fields. Due to the ambipolar potential in the plasma and the dc voltage in the dc and rf sheaths, the heating zone near the plasma–sheath interface is accessible only for high energy electrons that are able to overcome the repelling dc potential. Heated by the strong rf electric field, high energy electrons diffuse into the plasma bulk with a weak electric field and cause an intense ionization there. Low energy electrons originated in the ionization process are trapped by the ambipolar potential and are unable to penetrate into the heating zone. Their temperature is determined mainly by electron-electron collisions with hot electrons. The intense ionization by hot electrons together with a reduced plasma loss to the wall (proportional to the ion sound speed for cold electrons, $v_s = (T_{e1}/M)^{1/2}$), results in an enhanced plasma density and therefore, in reduction of electric field ($E \sim J/n$) compared to that in the bulk heating mode.

The transition of a CCP into the sheath heating mode (frequently called stochastic heating mode) has a threshold-like nature [1-3, 55]. The shift of electron heating to the plasma boundaries causes cooling of low energy electrons. This leads to an increase in the plasma density and hence to a reduction of the rf field in the plasma bulk, which results in more electron cooling. The electron-electron interaction between high and low energy electrons prevents a temperature collapse of cold electrons and limits the plasma density growth [55].

Strong non-equilibrium conditions for a CCP in the sheath heating mode may result in an abnormal dependence of both the effective electron temperature $T_{\text{eff}} = 2/3[\varepsilon] = 1/3 m[v_e^2]$ and plasma density on gas pressures [1]. This is illustrated in Fig. 5, where, starting at low pressures, $\langle \varepsilon(p) \rangle$ is growing while $n(p)$ is falling with gas pressure. In contrast, under equilibrium conditions, when EEDF is locally coupled with the heating electric field, these dependencies are reversed.

Another kind of strong non-equilibrium conditions occurs for CCP in the γ -mode at relatively high gas pressures and high rf voltages in the electrode sheaths [51, 52]. In the γ -mode, an avalanche of high energy electrons originating in the rf sheaths causes an intense ionization which is accompanied by a sharp rise in the

plasma density and by a sharp fall in both the electric field and the electron temperature in the plasma bulk. The evolutions of the EEPF, and the discharge and plasma parameters during the transition of a CCP into the γ -mode are shown in Figs. 6 and 7, [52]. The EEPF, T_{eff} , n , the discharge power and the discharge voltage are presented as functions of the discharge current density J for a 6.7 cm gap CCP in helium gas at 0.3 Torr. The dynamic resolution of the EFDF measurements (usually 3-4 orders of magnitude) is not sufficient to resolve the small amount of high energy electrons injected from the rf sheaths. Starting with $J = 1 \text{ mA/cm}^2$, which corresponds to a discharge voltage of about 100 V, the discharge transits from a nearly equilibrium α -mode dominated by volume heating into the γ -mode, when EEPF develops a low energy peak, with a sharp fall in T_{eff} and a steep rise in the plasma density. In the well-developed γ -mode (J around 10 mA/cm^2), the electron temperature is of an order of magnitude smaller, and the plasma density is of two orders of magnitude larger than the corresponding values in the low power α -mode.

Plasma characteristics of a CCP in the γ -mode are very close to those in the negative glow of a dc discharge, although in the first case the discharge is driven by an rf current, while in the second case, it is driven by a dc current. In both cases, an avalanche of fast electrons develops in the high voltage electrode sheath and produces ionization in neighboring plasma having low electron temperature. Similarly to a dc glow discharge, the lowest T_e in the γ -mode (close to the room temperature) was found in helium, where additional electron cooling via electron-atom elastic collisions is significant because of a relatively large m/M ratio. Fig. 8 shows the electron temperature as a function of pressure for helium in a well-developed γ -mode with a strongly non-equilibrium EEDF [50].

5. Non-equilibrium EEDF in ICP

A non-equilibrium two-temperature structure of the EEDF in the elastic energy range can also be found in an ICP. The absence of high voltage rf sheaths and the presence of a high plasma density in an ICP tend to prevent the formation of a two-temperature EEDF. On the other hand, in an ICP with anomalous skin effects where the rf current is not a local function of the rf field ($J \neq \sigma_p E$), ($\omega < v_T/\delta$ and $\delta < v_T/v$, where $v_T = (T_e/m)^{1/2}$ is the electron thermal velocity), collisionless selective electron heating of high energy electrons may cause the formation of a low energy peak of the EEDF, [53, 54, 56].

Collisionless electron heating occurs in an ICP when an electron crosses the skin layer in a fraction of the rf period, $v_T/\delta > \omega$. This means that only fast electrons ($\epsilon > \epsilon_t \approx \frac{1}{2}m(\delta\omega)^2$ where ϵ_t is the threshold energy) can effectively gain energy, while slow electrons ($\epsilon < \epsilon_t$), quiver without collisions in the skin layer (as in uniform rf fields) with no energy gain. The preferential heating of fast electrons together with the plasma ambipolar potential that keeps low energy electrons trapped outside the skin layer, causes the formation of the low energy electron group.

Figs. 9 and 10 show EEPFs measured in the midplane on the axis of an ICP in argon at 1 and 10 mTorr for three different frequencies: 3.4; 6.8 and 13.56 MHz and three different discharge powers: 12; 50 and 200 W, [53]. Observe that the low energy electron group is well pronounced at high rf frequencies and low discharge powers (plasma density). A flattening in the slope of the EEPF reflects electron heating and starts at higher electron energies for higher rf frequencies. At 1 mTorr and 12 W shown in Fig. 9, the calculated values of ϵ_t for frequencies 3.4; 6.8 and 13.56 MHz are 0.65; 2.5 and 9 eV respectively, which is in qualitative agreement with the experiment. For larger plasma densities and lower electron temperatures, strong electron-electron collisions ($v_{ee} \sim nT_e^{-3/2}$) force the EEPF to become Maxwellian. This is illustrated in Fig. 10 for 10 mTorr, 200 W, where

the electron temperature is lower and the plasma density is essentially higher than the corresponding values at 1 mTorr.

Another kind of a non-equilibrium is observed in an ICP operated in a nonlinear regime where the rf Lorentz force F_L acting on the electrons in the skin layer is large compared to the rf electric field force F_E , $F_L > F_E$. Such a condition is met at low driving frequencies when the rf magnetic field sustaining the ICP, $B \approx -E/\delta\omega$, is large and the corresponding cyclotron frequency satisfies the relationship $\omega_B > (\omega^2 + \nu^2)^{1/2}$. In this regime, a time averaged (ponderomotive) force F_p acts on the electrons in the non-uniform electromagnetic field of the skin layer, $F_p \sim \nabla E^2 \sim |\mathbf{J} \times \mathbf{B}|$, [33,34]. The reduction of a local rf current due to its spatial dispersion caused by electron thermal motion, leads to a reduction of the ponderomotive force acting on fast electrons. Therefore, low energy electrons appear to be affected by the ponderomotive force to a larger extent than high energy electrons [35]. This results in a depletion of EEPF by low energy electrons in the skin layer [57].

Fig. 11 shows EEPFs measured at different distances from the Quartz window adjacent to an rf coil in a low frequency ICP for two radial positions, [57]: at $r = 4$ cm corresponding to the maximum of the rf field radial distribution, and at $r = 0$ where $E = 0$ and $F_p = 0$. In the upper part of Fig. 11, the EEPF is measured at $r = 4$ cm, and in the lower part, it is measured at $r = 0$; on the left of Fig. 11, the EEPF is measured between the window ($z = 0$) and the position of maximal plasma density ($z = 5.5$ cm), and on the right, it is measured between $z = 5.5$ cm and the chamber bottom $z = 10.5$ cm. Depletion in the low energy part of the EEPF measured in the skin layer is clearly seen near the window, while the EEPFs measured in the right part of the chamber and at its axis (where the rf field is negligible) are not depleted by low energy electrons. Those EEPFs are the same for the total electron energy $\varepsilon = \frac{1}{2}mv_e^2 + e\phi$, while EEPFs affected by the ponderomotive force, shown in the upper left part of Fig. 11, are the same for the total electron energy $\varepsilon = \frac{1}{2}mv_e^2 + e\phi + e\phi_p$ that includes the ponderomotive potential ϕ_p defined by the relationship $F_p = -e\nabla\phi_p$.

6. EEDF control in gas discharge plasma

In steady state low pressure discharges with a uniform or a weakly non-uniform electric field, where the electric field and the EEDF are nearly in equilibrium, the effective electron temperature is determined by the ionization process, resulting in $T_{\text{eff}} = T_{\text{eff}}(p\Lambda)$, while the electron energy losses define the heating electric field. For this reason, different discharges with different electron heating mechanisms usually have similar EEDF and T_{eff} , for specified $p\Lambda$ and P_d . In a strongly non-equilibrium state attained in discharges with strong non-uniform heating fields and enhanced population of low energy electrons, the effective electron temperature can be lower than in discharges at equilibrium for given $p\Lambda$ and P_d . Let us consider just few examples of possible electron temperature control in non-equilibrium rf plasmas.

The plasma density n and the mean electron energy $[\varepsilon] = 3/2 \cdot T_{\text{eff}}$ in a CCP, found as appropriate integrals of the measured EEPF for a CCP presented in Fig. 3, are given in Fig. 5 as functions of argon pressure. At relatively high pressures ($p > 0.5$ Torr), when the volume electron heating dominates, the mean electron energy is close to that in a dc positive column, and drops slightly as the argon pressure increases, while the plasma density grows. Those trends are common for discharges that are in equilibrium with the heating electric field. At low pressures ($p < 0.5$ Torr), the discharge transits to the sheath heating mode, and the plasma is no longer in equilibrium with the rf field. In this non-equilibrium mode, the mean electron energy $[\varepsilon(p)]$ and the plasma density $n(p)$ dependencies are reversed; the effective electron temperature is essentially lower while the plasma density is larger than is expected at the equilibrium. Stimulating the CCP transition to the sheath-heating mode (via

pressure reduction or increase in the discharge power), one may significantly reduce the electron temperature and enhance (or suppress) desirable plasma-chemical processes.

Another example of EEDF control is through the variation of the rf frequency in a low pressure ICP with anomalous skin effect (see Figs. 9 and 10). Fig. 12 shows the dependence of the effective electron temperature (corresponding to the EEPF from Fig. 9) on the frequency for different discharge powers. At low discharge powers (plasma density) when the electron-electron collision rate is not sufficiently high to destroy the two-temperature EEPF structure, a four-fold increase in the frequency leads close to a two-fold reduction in the electron temperature. The effect of the frequency diminishes when the plasma density increases, and for sufficiently high plasma densities, the electron-electron collisions bring the EEDF to a Maxwellian distribution, where the electron temperature is determined only by the $p\Lambda$ product, in spite of the fact that the EEDF is not in a local equilibrium with the non-uniform rf field.

Decoupling of electron heating from the electron energy loss process (which is typical for non-equilibrium) can be achieved “artificially” in a pulse-operated discharge, when during a short pulse-on time $\tau_{\text{on}} \ll z^{-1}$, the effective electron temperature T_{eff} overshoots its steady state value T_e^0 , $T_{\text{eff}} > T_e^0$. Then, in the afterglow (pulse-off) stage, due to inelastic collisions and fast electron escape to the wall, the electron temperature quickly drops to a level lower than T_e^0 and finally slowly approaches the gas temperature. The electron temperature may even become lower than the gas temperature, because of the diffusion cooling [58-60].

This is illustrated in Fig. 13 where the electron temperature evolution is shown for different argon pressure, in the afterglow stage of argon ICP maintained at 4 MHz with an internal coil having a ferromagnetic core [61]. The values of the electron temperature for the initial CW mode at different argon pressure are inserted in Fig. 13. T_e was calculated as appropriate integral of the measured EEDFs. Observe that electron cooling is faster for lower gas pressures, suggesting that the diffusion cooling is the main mechanism of the electron energy loss in the afterglow [58]. Electron temperature cooling occurs more rapidly at lowest gas pressures, as plasma loss to the wall transits from the collisional ambipolar diffusion regime at high pressures to the Tonks-Langmuir regime at low pressures, controlled by the ion inertia. In the late afterglow stage, T_e reaches very low values (down to 0.05 eV at 3 mTorr), which are close to the argon gas temperature.

The large span of the electron temperature change during the afterglow suggests that the electron temperature can be controlled in the periodically-pulsed discharge by varying the off-cycle time τ_{off} . Since the pulse-on stage is usually much shorter than the pulse-off, afterglow stage, the time averaged electron temperature in a periodically pulsed discharge is lower than in a steady state discharge.

Time evolutions of EEPF and corresponding plasma parameters measured in a periodically pulsed ICP [61] are shown in Figs. 14 and 15. The measurement were performed in the ICP afterglow stage (between $t = 2.8 \mu\text{s}$ and $t = 20 \mu\text{s}$) with $\tau_{\text{on}} = 2 \mu\text{s}$ at 550 W pulsed power corresponding to 50 W of the averaged discharge power. The EEPFs corresponding to different afterglow time have been shifted in Fig. 14 to higher energy for clarity of presentation. The EEPF shift in the energy is equal to the plasma potential variation in time. Due to the absence of the electric field and a reduced electron temperature, the EEPF in the late afterglow stage is Maxwellian. The lowest electron temperature in the afterglow stage is controlled by the afterglow duration. During the afterglow stage, there is a twofold drop in the plasma density and a fourfold drop in the electron temperature, reaching an order of magnitude lower value than that in the CW mode. The time averaged electron temperature in the afterglow stage ($\langle T_e \rangle \approx 0.9 \text{ eV}$) is fivefold decreased, while the averaged plasma density ($\langle n \rangle \approx 4.5 \cdot 10^{11} \text{ cm}^{-3}$) is threefold increased compared to the corresponding values measured in the CW mode ($T_e = 4.4$

eV and $n = 1.5 \cdot 10^{11} \text{ cm}^{-3}$) for the same discharge power of 50 W. The reason for such significant difference in the plasma density is the intense ionization (plasma production) by the “overheated” electrons during the on-cycle, and reduction (due to electron cooling) in plasma diffusion to the wall in the afterglow stage.

In the periodically pulsed discharge, the reduction in the time-averaged electron temperature is accompanied by the presence of high temperature electrons during the on-cycle. Their effective electron temperature is expected to be higher than at the equilibrium in the CW mode, because during the on-cycle, the electric field is higher than in the CW mode. Due to an excess of high energy electrons during the on-cycle, and their fast cooling during the off-cycle (afterglow), the time averaged EEPF in a periodically pulsed discharge is expected to have a two-temperature structure, like the bi-Maxwellian EEPF in a low pressure CCP. Since the ionization rate dependence on the electron temperature is nearly exponential, the electron temperature (electron mean energy) during the pulse on-cycle experiences just a moderate increase compared to T_e in the CW mode. Therefore, in a typical case of a periodically pulsed plasma when a temporal non-equilibrium between ionization and particle loss occurs ($\tau_{\text{off}} \gg \tau_{\text{on}}$), the effective electron temperature, averaged over the period ($\tau_{\text{on}} + \tau_{\text{off}}$), is always lower than T_e in the CW mode.

The possibility of modifying plasma parameters modification in capacitive and inductive rf discharges by injection of a high energy electron beam produced outside the plasma has been demonstrated in [62,63]. It has been shown that injection of high energy electrons ($\epsilon_b \approx 100 \text{ eV}$) significantly (few times) decreased plasma potential and the electron temperature and increased the plasma density. The model based on the ionization and energy balance of bounded gas discharge plasma developed by these authors was found in close agreement with experimental observations.

A spatially non-equilibrium plasma with cold electrons can be created by dividing the discharge chamber by a negatively biased mesh (grid) [64, 65]. Due to its high negative potential V_G , the mesh repels all electrons with energy ϵ less than eV_G , where V_G is referenced to the first, active (with heating electric field) plasma sub-chamber. Therefore, only a small portion of fast electrons with $\epsilon > eV_G$ can penetrate the second, passive (without heating electromagnetic field) sub-chamber. Due to ionization in the second sub-chamber performed by the fast electrons, a population of low energy electrons is created there. A potential barrier created by the mesh prevents an exchange between electrons in both sub-chambers, and therefore, without a heating field, the electrons in the second sub-chamber remain cold. Their temperature is determined by the balance between their heating via electron-electron collisions with primary fast electrons and diffusion cooling.

Using a coarse mesh with openings much larger than the Debye length, and changing the sheath width around the mesh wire with the mesh potential, one can change the mesh opacity for the middle energy electrons (in the first sub-chamber) and for the low energy electrons (in the second sub-chamber), thus mixing electrons of both sub-chambers. As a result, the electron temperature in the second sub-chamber can be smoothly changed by varying the mesh potential. This was illustrated in Ref. 64, where the electron temperature in the second sub-chamber has been reduced up to two orders of magnitude, while the plasma density has been increased an order of magnitude. The increase in the plasma density n_{eII} is a direct consequence of the drop in the electron temperature T_{eII} that slows down the plasma diffusion to the wall.

An additional plasma parameter control in the plasma source with dividing mesh was demonstrated in Ref. 66, where an enhancement in the plasma density (1-2 orders of magnitude) in the second sub-chamber was achieved with its positive biasing with respect to the first sub-chamber. In that case, the first sub-chamber operated as a

plasma cathode, while the bias voltage accelerated the electrons escaping through the mesh from the first sub-chamber, and thus significantly increased their ionizing ability in the second sub-chamber.

One way to control the high energy tail of EEDF in argon ICP afterglow plasma without significant change in the bulk electron temperature and plasma density has been demonstrated in Ref. 67. The EEDF tail modification has been achieved by biasing a small electrode near the plasma boundary with a negative (reference to the plasma) dc potential $-V$. At nonlocality condition, by collecting plasma electrons to the electrode, one can globally deplete the EEDF with electrons whose energies exceed the electrode potential ($\epsilon > eV$).

Another way to control the high energy tail of the EEDF demonstrated in Ref. 67 was quenching of argon excited states with the addition of a small amount of nitrogen gas. In the afterglow stage, the high energy electrons are produced in reactions with excited metastable argon atoms. Therefore, the quenching of metastable atoms reduces the population of fast electrons.

The possibility to achieve a non-equilibrium state is to create artificially a strong spatial non-uniformity in the electric field. Such possibility was studied for the positive column of a dc discharge by forcing the discharge current to flow through a narrow orifice at the condition $\lambda_e \approx \Lambda$, [69]. It has been shown that the electric field, the mean electron energy and the plasma density significantly increase in the vicinity of the orifice, compared to their corresponding values in the undisturbed part of the positive column. Concurrently, some reduction in the mean electron energy (compared to its unperturbed value) and a field reversal were observed in the adjacent plasma.

7. Conclusions

In steady-state bounded gas discharge plasmas, at near E/F-equilibrium conditions, ionization and electron energy balance determine the effective electron temperature T_{eff} and the plasma density n as universal functions of the $p\Lambda$ -product and the discharge power P_d , and those functions are practically independent of the particular mechanism of electron heating process. The relationships $T_{\text{eff}}(p\Lambda)$ and $n(p\Lambda, P_d)$ may change under the condition of strong non-locality when $\lambda_e \gg \Lambda \gg \delta$. In general, in low pressure discharges sustained by a non-uniform electromagnetic field at $\lambda_e > \Lambda$, the EEDF is not in a local equilibrium with the heating field. For such a non-equilibrium condition, the EEDF is in integral equilibrium with the spatially averaged electromagnetic field. In this case, electrons gain energy in the area of a strong field, and, because of their thermal motion, transfer this energy to the area of a weak field. In this respect, low pressure discharges at $\lambda_e > \Lambda$ or/and $\omega > \xi$ resemble non-self-sustained plasmas, where electron heating and plasma parameters are shifted in space or/and in time, and $df_e(\epsilon)/dr = 0$ or/and $df_e(\epsilon)/dt = 0$ in the limit $\lambda_e \gg \Lambda$ or/and $\omega \gg \xi$.

The non-equilibrium considered above, is associated with electron heating in a non-uniform field in glow discharge, CCP and ICP, may occur in others types of rf discharges such as helicon, surface wave and ECR plasmas. Low electron temperatures ($T_e = 0.6-1.3$ eV), significantly lower than those expected for plasmas in equilibrium with the rf field, have been found in distributed ECR plasma sources, having an array of dipole magnets, energized at 2.45 GHz in hydrogen at 1-4 mTorr [69].

The degree of non-equilibrium leading to space separation between electron energy gain and EEDF in locally non-equilibrium plasmas is different for different kinds of discharges. The strongest non-equilibrium is in the cathode glow of dc glow discharges and in the capacitive rf discharge in the γ -mode, where strong electric fields

(dc or/and rf) are present in the electrode sheath, and an avalanche of fast electrons is developing there, causing an intense ionization and significant drop in electron temperature in the adjacent plasma. Some lesser effect is observed in the capacitive rf discharge in the α -mode and even lesser, in inductive plasma.

The localization of electron heating in a narrow zone is not sufficient to achieve strong non-equilibrium plasma with two distinctive groups of electrons (like a nearly bi-Maxwellian EEDF). At low gas pressures, when non-local electron kinetics dominates ($\lambda_e \gg \Lambda$), the plasma parameter space distribution is insensitive to the rf field distribution, unless there is some segregation mechanism that prevents low energy electrons heating and mixing with high energy electrons.

In bounded plasmas with intrinsically non-uniform plasma density, the ambipolar potential $\phi \sim (T_e/e)\ln(n/n_0)$, where n_0 is the maximal plasma density corresponding to $\phi = 0$, keeps low energy electrons trapped in the vicinity of the plasma center, preventing them from reaching the plasma boundary where the heating takes place. In dc glow and capacitive rf discharges, the existence of high voltage sheaths with strong electron heating (and electron multiplication) and strong dc field, makes the segregation of low energy electrons even more thorough. For this reason, the most expressed two-temperature structure in EEDF with the lowest electron temperature (close to room temperature) is observed in dc glows and in CCPs in the γ -mode. The segregation function also can be performed with a dc magnetic field, as presumably is the case for a non-equilibrium ECR plasma source [69].

In non-equilibrium conditions with two-temperature EEDF, low energy electrons are usually heated by high energy electrons via electron-electron collisions. For sufficiently high plasma density, the temperatures of low and high energy electron groups equalize and EEDF tends to a Maxwellian distribution, independent of the existence of a segregation barrier or of the selective heating of particular part of EEDF by the electromagnetic field.

A high level of non-equilibrium conditions with essentially different electron temperatures of low and high energy electron groups of the EEDF can be attained artificially by spatial or time concentration of the electron heating field in the presence of some effective segregation mechanism. In pulse discharges, the non-equilibrium is provided by the absence of the heating field and fast disappearance of fast electrons in the afterglow stage. In discharges with artificial spatial concentration of electron heating, some segregation barrier separating the low and high energy electrons is needed to achieve a EEDF dominated by low energy electrons. Creation of such systems with the ability to control electron energy is a challenge for future application of gas discharge plasmas.

References

1. V. Godyak and R. Piejak, Abnormally low electron temperature and heating mode transition in a low pressure argon rf discharge at 13.56 MHz, *Phys. Rev. Lett.* **65**, 996 (1990).
2. A. S. Smirnov and L. D. Tsendin, The space-time-averaging procedure and modeling of the rf discharge, *IEEE Trans. Plasma Sci.* **19**, 130 (1991).
3. I. D. Kaganovich and L. D. Tsendin, Space-time-averaging procedure and modeling of the rf discharge, part II: modeling of collisional low-pressure rf discharge, *IEEE Trans. Plasma Sci.* **20**, 66 (1992).
4. V. A. Godyak and R. B. Piejak, Paradoxical spatial distribution of the electron temperature in a low pressure rf discharge, *Appl. Phys. Lett.* **63**, 3137 (1993).
5. V. I. Kolobov and V. A. Godyak, Nonlocal electron kinetics in collisional gas discharge plasmas, *IEEE Trans. Plasma Sci.* **23**, 503 (1995).
6. L. D. Tsendin, Electron kinetics in non-uniform glow discharge plasmas, *Plasma Source Sci. Technol.* **4**, 200 (1995).
7. U. Kortshagen, I. Pucropskiy and L. D. Tsendin, Experimental investigation and fast two-dimensional self-consistent kinetics modeling of a low-pressure inductively coupled rf discharge, *Phys. Rev. E* **51**, 6063 (1995).
8. U. Kortshagen, C. Busch and L. D. Tsendin, On simplifying approaches to the solution of the Boltzmann equation in a spatially inhomogeneous plasmas, *Plasma Source Sci. Technol.* **5**, 1 (1996).
9. S. V. Berezhnoi, I. D. Kaganovich and L. D. Tsendin, Fast modeling of low-pressure radio-frequency collisional capacitively coupled discharge and investigation of the formation of a non-Maxwellian electron distribution function, *Plasma Sources Sci. Technol.* **7**, 268 (1998).
10. U. Kortshagen and L. Tsendin, eds. *Electron Kinetics and Application of Glow Discharges*, New York: Plenum (1998).
11. L. D. Tsendin, Current trend in electron kinetics of gas discharge, *Plasma Sources Sci. Technol.* **12**, S51 (2003).
12. V. Godyak, Statistical heating of electrons at oscillating plasma boundary, *Soviet Physics-technical physics* **16**, 1073 (1972).
13. V. Godyak, Steady-state low pressure rf discharge, *Soviet J. Plasma Physics* **2**, 78 (1976).
14. V. Godyak, O. Popov and A. Ganna, Effective electron collision frequency in rf discharge, *Sov. J. Plasma Phys.* **3**, 560 (1976).
15. M. M. Turner, Phys. Collisionless heating in an inductively coupled discharge, *Rev. Lett.* **71**, 1844 (1993).
16. V. A. Godyak, R. B. Piejak and B. M. Alexandrovich, Electrical characteristics and electron heating mechanism of an inductively coupled rf discharge, *Plasma Sources Sci. Technol.* **3**, 161 (1994).
17. V. Godyak, Electron kinetic and electrodynamic characteristics of ICP in stochastic heating regime, in *Electron kinetics and Application of Glow Discharges*, edited by U. Kortshagen and L. D. Tsendin, p. 241, Plenum, New York (1998).
18. M. Lieberman and V. Godyak, From Fermi acceleration to collisionless discharge heating, *IEEE Trans. Plasma Sci.* **26**, 955 (1998).
19. G. Gozadinos, M. M. Turner and D. Vender, Collisionless electron heating by capacitive rf sheaths, *Phys. Rev. Lett.* **87**, 135004 (2001).
20. I. D. Kaganovich, Effect of collisions and particle trapping on collisionless heating, *Phys. Rev. Lett.* **82**, 327 (1999).
21. I. D. Kaganovich, O. V. Polomarov and C. E. Theodosiou, Landau damping and anomalous skin effect in low-pressure gas discharges: self-consistent treatment of collisionless heating, *Phys. Plasmas* **11**, 2399 (2004).
22. V. A. Godyak, Hot plasma effects in gas discharge plasma, *Phys. Plasmas* **12**, 055501 (2005).
23. O. V. Polomarov, C. E. Theodosiou and I. D. Kaganovich, Enhanced collisionless heating in a nonuniform plasma at the bounce resonance condition, *Phys Plasmas* **12**, 080704 (2005).
24. I. D. Kaganovich, Revisiting the anomalous rf field penetration into warm plasma, to be published in *IEEE Trans Plasma Sci.*
25. V. Godyak, *Soviet Radio Frequency Discharge Research*, Delphic Ass., Inc., Falls Church, VA (1986).
26. M. A. Lieberman, Analytical solution for capacitive rf sheath, *IEEE Trans. Plasma Sci.* **16**, 638 (1988).
27. M. A. Lieberman, Dynamics of a collisional, capacitive rf sheath, *IEEE Trans. Plasma Sci.* **17**, 338 (1989).
28. V. Godyak and N. Sternberg, Dynamic model of the electrode sheaths in symmetrically driven rf discharges, *Phys. Rev. A* **42**, 2299 (1990).

29. R. H. Cohen and T. D. Rognlien, Electron kinetics in radio-frequency magnetic fields of inductive plasma sources, *Plasma Sources Sci. Technol.* **5**, 442 (1996).
30. R. H. Cohen and T. D. Rognlien, Induced magnetic-field effects in inductively coupled plasmas, *Phys. Plasmas* **3**, 1839 (1996).
31. V. Godyak, R. Piejak and B. Alexandrovich, Observation of second harmonic currents in inductively coupled plasmas, *Phys. Rev. Lett.* **83**, 1610 (1999).
32. A. Smolyakov, V. Godyak and A. Duffy, On nonlinear effects in inductively coupled plasmas, *Phys. Plasmas* **7**, 4755 (2000).
33. V. Godyak, R. Piejak B. Alexandrovich and A. Smolyakov, Observation of the ponderomotive effect in an inductive plasma, *Plasma Sources Sci. Technol.* **10**, 459 (2001).
34. F. F. Chen, Collisional, magnetic, and nonlinear skin effect in radio-frequency plasmas, *Phys. Plasmas* **8**, 3008 (2001).
35. A. Smolyakov, V. Godyak and Y. Tychetskiy, Effect of electron thermal motion on the ponderomotive force in inductive plasma, *Phys. Plasmas* **8**, 3857 (2001).
36. M. A. Lieberman and A. J. Lichtenberg, *Principles of Plasma Discharges and Materials Processing*, New York: Wiley (1994).
37. V. A. Godyak, Soviet Radio Frequency Discharge Research, Delphic Associates Inc, Falls Church, VA (1986).
38. C. Beneking, Power dissipation in capacitively coupled rf discharges, *J. Appl. Phys.* **68**, 4461 (1990).
39. V. A. Godyak, R. B. Piejak and B. M. Alexandrovich, Ion flux and ion power losses at the electrode sheaths in a symmetrical rf discharge, *J. Appl. Phys.* **69**, 3455 (1991).
40. A. I. Morozov and V. Savelyev, *Reviews of Plasma Physics* (Kluwer Academic/Plenum Publishers, New York, Vol. 21 (2000) p.206.
41. Y. Raitses, D. Staack, A. Smirnov and N. J. Fisch, Space charge saturated sheath regime and electron temperature in Hall thrusters, *Plasmas* **12**, 073507 (2005)
42. N. Hershkowitz, J. Ding, R. A. Breun, R. T. S. Chen, J. Mayer and A. K. Quick, Does high density low pressure etching depend on the type of plasma source, *Phys. Plasmas* **3**, 2197 (1996).
43. G. Lister, Y. Li and V. Godyak, Electrical conductivity in high frequency plasmas, *J Appl. Phys.* **79**, 8993 (1996).
44. R. W. Boswell and F. F. Chen, Helicons, the early years, *IEEE Trans. Plasma Sci.* **25**, 1229 (1997).
45. F. F. Chen and R. W. Boswell, Helicons, the past decade, *IEEE Trans. Plasma Sci.* **25**, 1245 (1997).
46. G. S. Solntsev, A. I. Orlov and B. A. Dovzhenko, Microwave field effect on plasma characteristics of the negative glow in a helium glow discharge, *Sov. Phys.-Techn. Phys* **38**, 893 (1970).
47. J. E. Lawler, E. A. Den Hartog and W. N. G. Hitchon, Power balance of negative-glow electrons, *Phys. Rev. A* **43**, 4427 (1991).
48. V. I. Kolobov and L. D. Tsendin, An analytic model of the cathode region of a short glow discharge in light gases, *Phys. Rev. A* **46**, 7837 (1992).
49. R. R. Arslanbekov and A. A. Kudryavtsev, Energy balance of the bulk, Maxwellian electrons in spatially inhomogeneous negative-glow plasmas, *Phys. Rev. E* **58**, 6539 (1998).
50. V. A. Godyak, R. B. Piejak and B. M. Alexandrovich, Measurement of the electron energy distribution in low pressure rf discharges, *Plasma Sources Sci. Technol.* **1**, 36 (1992).
51. V. Godyak and A. Khanneh, Ion bombardment secondary electron maintenance of steady rf discharge, *IEEE Trans. Plasma Sci.* **14**, 112 (1986)
52. V. A. Godyak, R. B. Piejak and B. M. Alexandrovich, Evolution of the electron energy distribution function during rf discharge transition to the high voltage mode, *Phys. Rev. Lett.* **68**, 49 (1992).
53. V. Godyak, R. Piejak and B. Alexandrovich, Electron Energy Distribution Function Measurements and Plasma Parameters in Inductively Coupled Argon Plasma, *Plasma Sources Sci. Technol.* **11**, 525 (2002).
54. V. Godyak and V. Kolobov, Effect of collisionless heating on electron energy distribution in an inductively coupled plasma, *Phys. Rev. Lett.*, **81**, 369 (1998).
55. S. V. Berezhnoi, I. D. Kaganovich and L. D. Tsendin, Generation of cold electrons in a low –pressure rf capacitive discharge as an analog of a temperature explosion, *Plasma Physics Reports* **24**, 603 (1998).
56. V. Godyak, EEDF in dense rf plasmas, ESCAMPIG 96, p. IX, European. Phys. Soc. Editors: Lukac, Kosinar, Skalny; Bratislava, Slovakia (1996).
57. V. Godyak, B. Alexandrovich and V. Kolobov, Lorentz force effect on the electron energy distribution in inductively coupled plasmas, *Phys. Rev. E* **64**, 026406 (2001).
58. M. A. Biondi, Diffusion cooling of electrons in ionized gases, *Phys. Rev.* **93**, 1136 (1954).
59. X. Tang and D. Manos, Time-resolved electrostatic probe studies of a pulsed inductively-coupled plasma, *Plasma Source Sci. Technol.* **8**, 594 (1999).
60. A. Mareska, K. Orlov and U. Kortshagen, Experimental study of diffusive cooling of electrons in a pulse inductively coupled plasma, *Phys. Rev. E* **60**, 056405 (2002).
61. V. A Godyak and B. M. Alexandrovich, Plasma parameter evolution in a periodically pulsed ICP, Proceedings of XXVIIth ICPIG, Report 06-390, Eindhoven, the Netherlands (2005).
62. F. A. Haas, A. Goodyear and N. St. J. Braithwaite, Tailoring of electron energy distributions in low temperature plasmas, *Plasma Sources Sci. Technol.* **7**, 471 (1998).

63. F. A. Haas, and N. St. J. Braithwaite, Tailoring of electron energy distributions in low-pressure inductive discharges, *Appl. Phys. Lett.* **74**, 338 (1999).
64. K. Kato, S. Iizuka and N. Sato, Electron-temperature control for plasmas through negatively biased grid, *Appl. Phys. Lett.* **65**, 816 (1994).
65. J. I. Hong, et al, Electron temperature control with grid bias in inductively coupled argon plasma, *Phys. Plasmas* **6**, 1917 (1999).
66. R. Ikada et al, Production of high density and low electron-temperature plasma by a modified grid-biasing method using inductively coupled rf discharge, *Thin Solid Films* **457**, 55 (2004).
67. C. A DeJoseph, V. I. Demidov and A. A. Kudryavtsev, Modification of nonlocal electron energy distribution in a bounded plasma, *Phys. Rev. E* **72**, 036410 (2005).
68. V. Godyak, R. Lagushenko and J. Maya, Spatial evolution of the electron energy distribution in the vicinity of a discharge tube constriction, *Phys. Rev. A* **38**, 2044 (1988).
69. A. A. Ivanov Jr, C Rouille, M. Bacal, Y. Arnal, S. Bechu and J. Pelletier, H-ion production in electron cyclotron resonance driven by multicusp volume source, *Rev. Sci. Instrum.* **75**, 1750 (2004).

Figure Captions

- Fig. 1. Plasma parameter profiles measured along an ICP in the axial direction.
- Fig. 2. EEPF's measured in the ICP at different axial positions.
- Fig. 3. EEPF evolution with argon pressure in a CCP at 13.56 MHz.
- Fig. 4. EEDF and EEPF in an argon CCP at 13.56 MHz and 100 mTorr.
- Fig. 5. Plasma parameters and ratio of stochastic, P_{st} to collisional, P_v power absorption in a CCP.
- Fig. 6. EEPF evolution with discharge current density in a helium CCP at 13.56 MHz and 0.3 Torr.
- Fig. 7. Plasma parameter evolution corresponding to Fig. 6.
- Fig. 8. Electron temperature in a CCP in the γ -mode; helium 0.3 Torr, 13.56MHz.
- Fig. 9. EEPF in an argon ICP at 1 mTorr and different discharge power: 12; 50 and 200 W.
- Fig. 10. EEPF in an argon ICP at 10 mTorr and different discharge power: 12; 50 and 200 W.
- Fig. 11. EEPF in a low frequency ICP at different axial positions.
- Fig. 12. Frequency dependence of electron temperature in an ICP at different discharge power: 12.5; 50 and 200 W.
- Fig. 13. Electron temperature in an argon ICP afterglow at different argon pressure.
- Fig. 14. EEPF in an argon ICP at different moments of afterglow time t .
- Fig. 15. Plasma parameters evolution in a periodically pulse ICP in the afterglow stage.

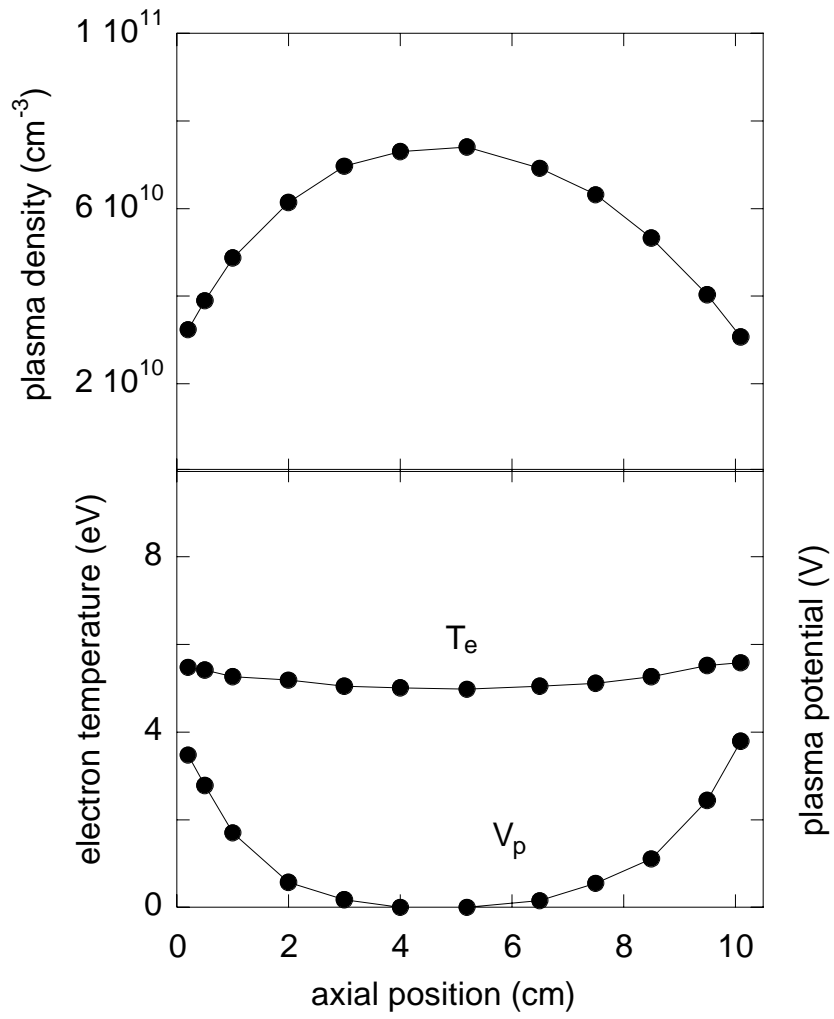


Fig. 1

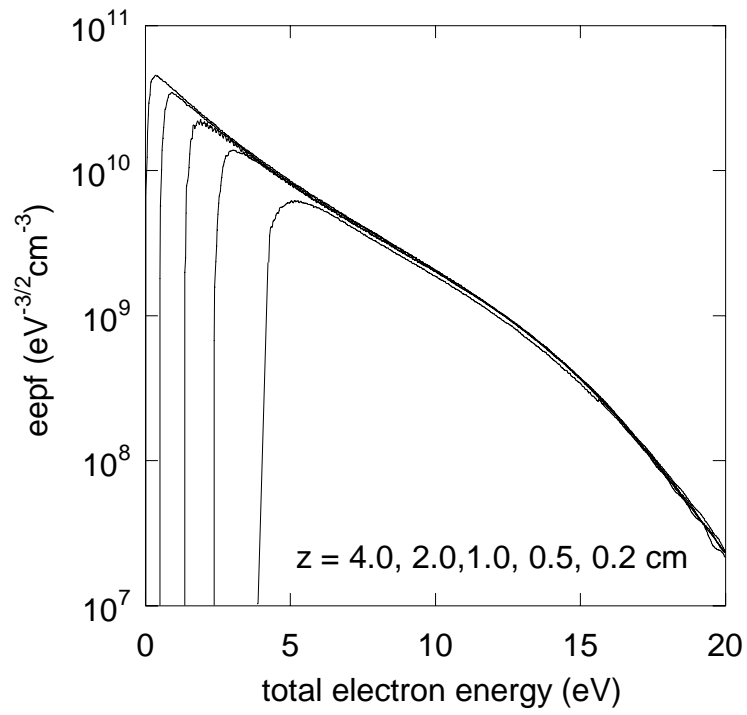


Fig. 2

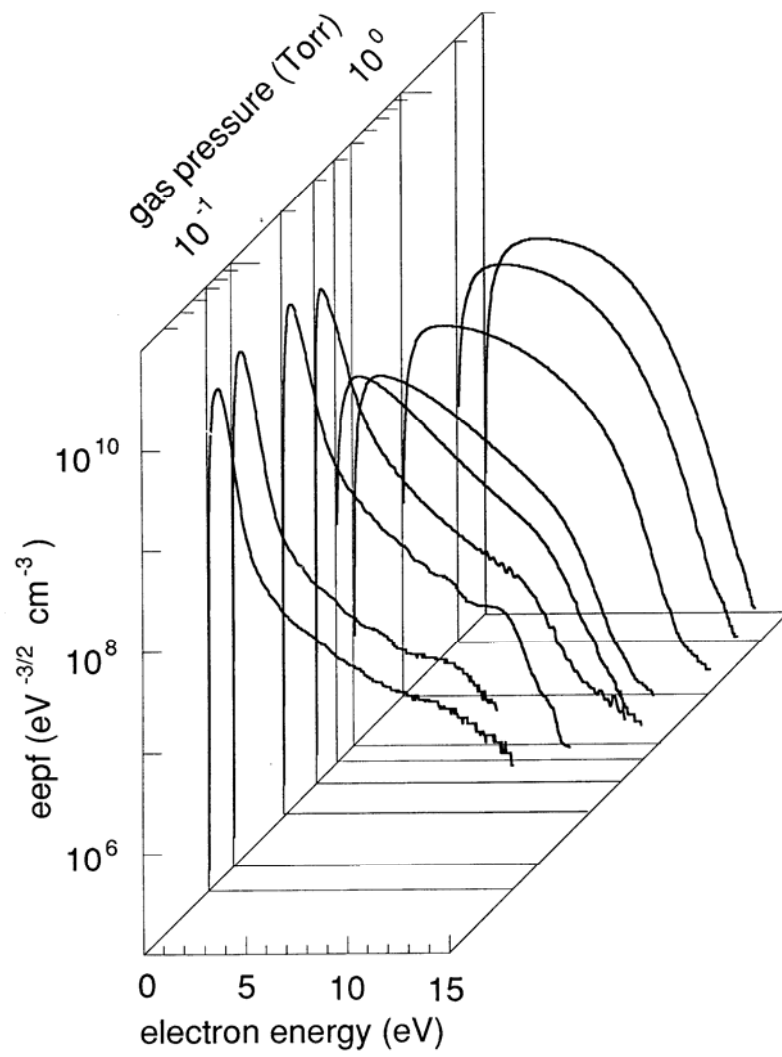


Fig. 3

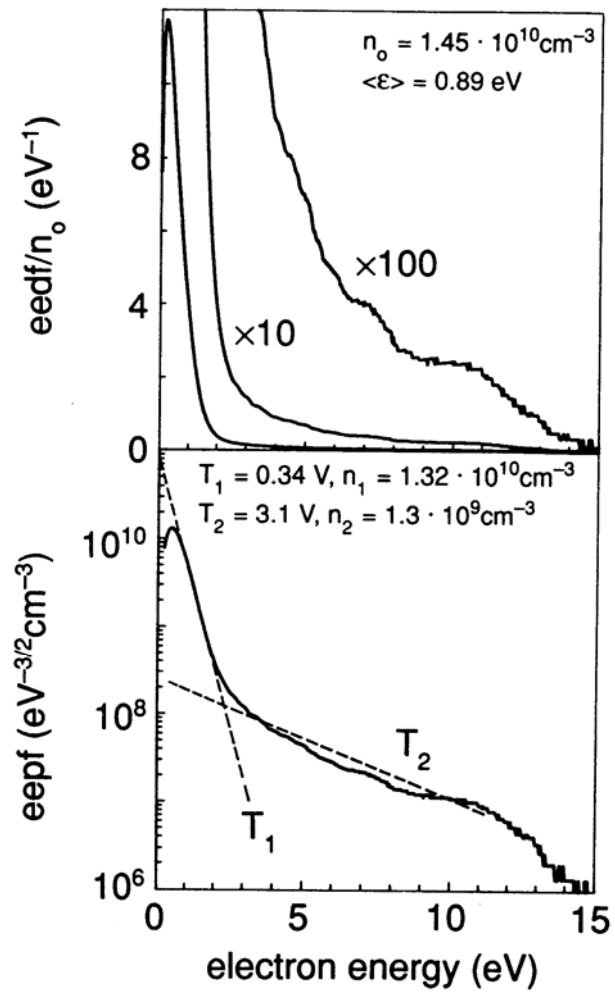


Fig. 4

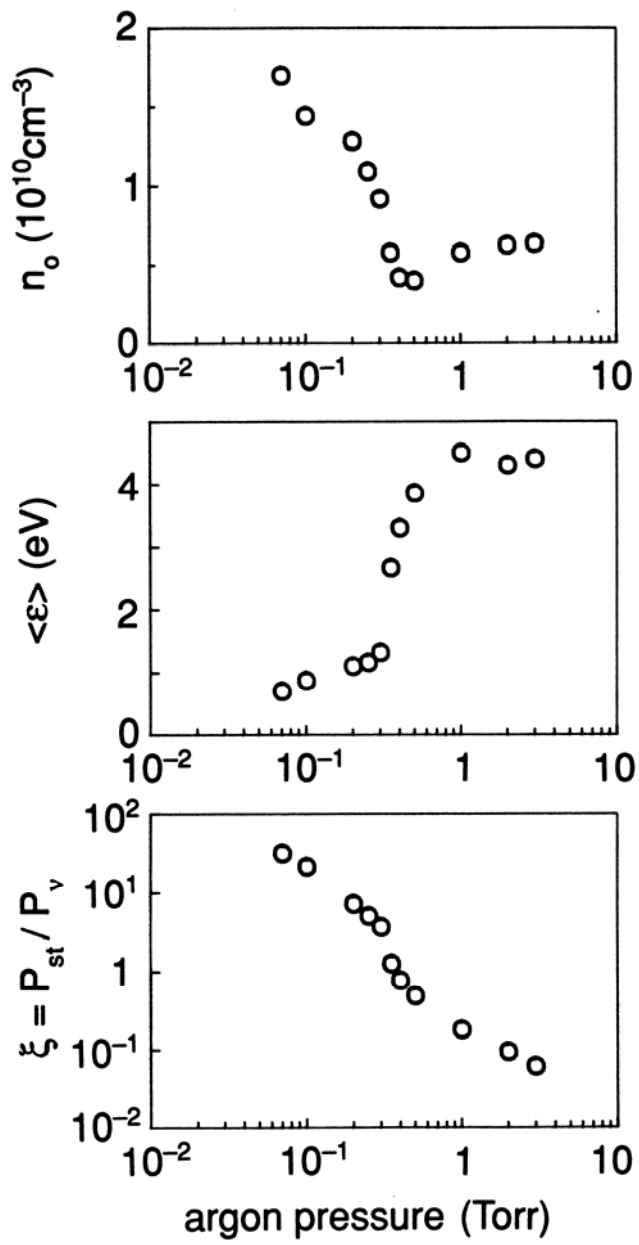


Fig. 5

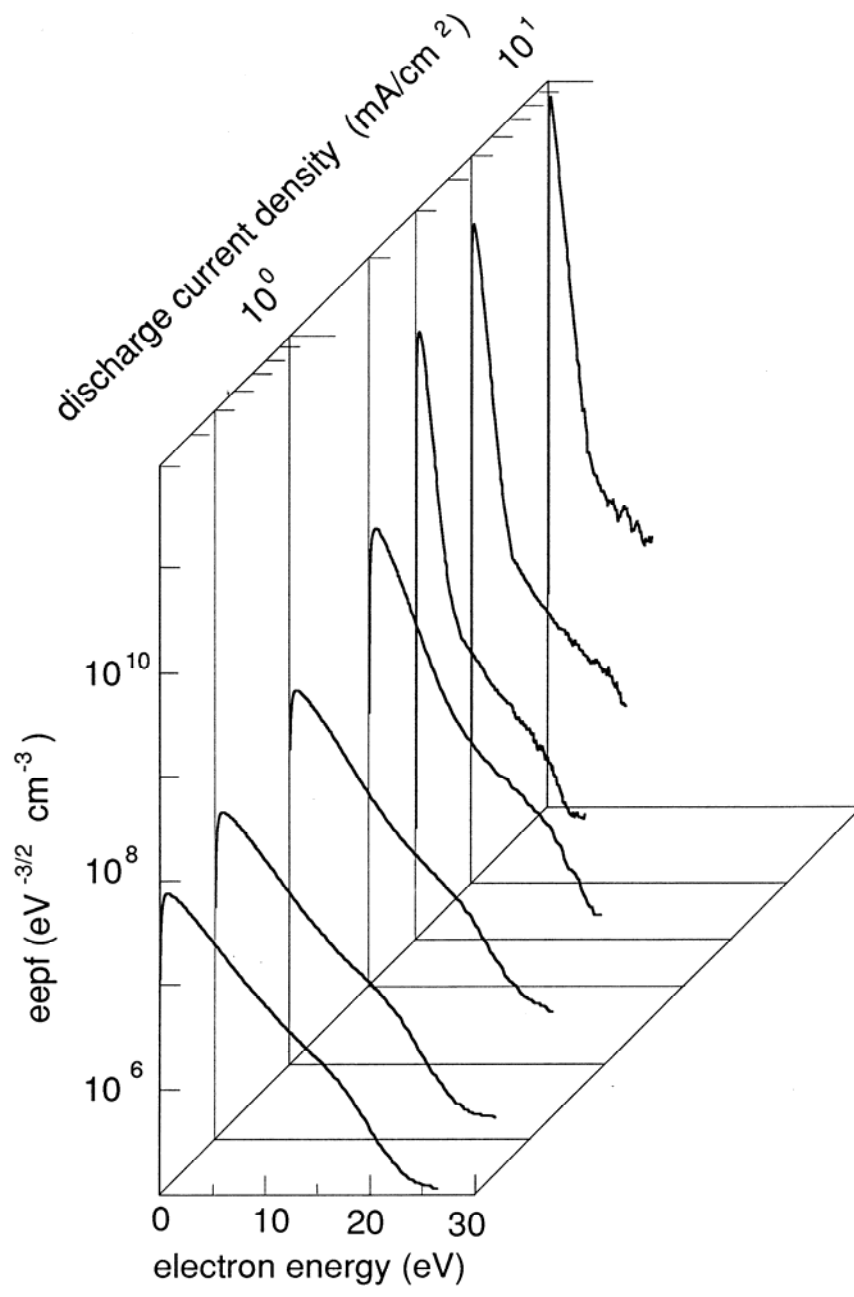


Fig. 6

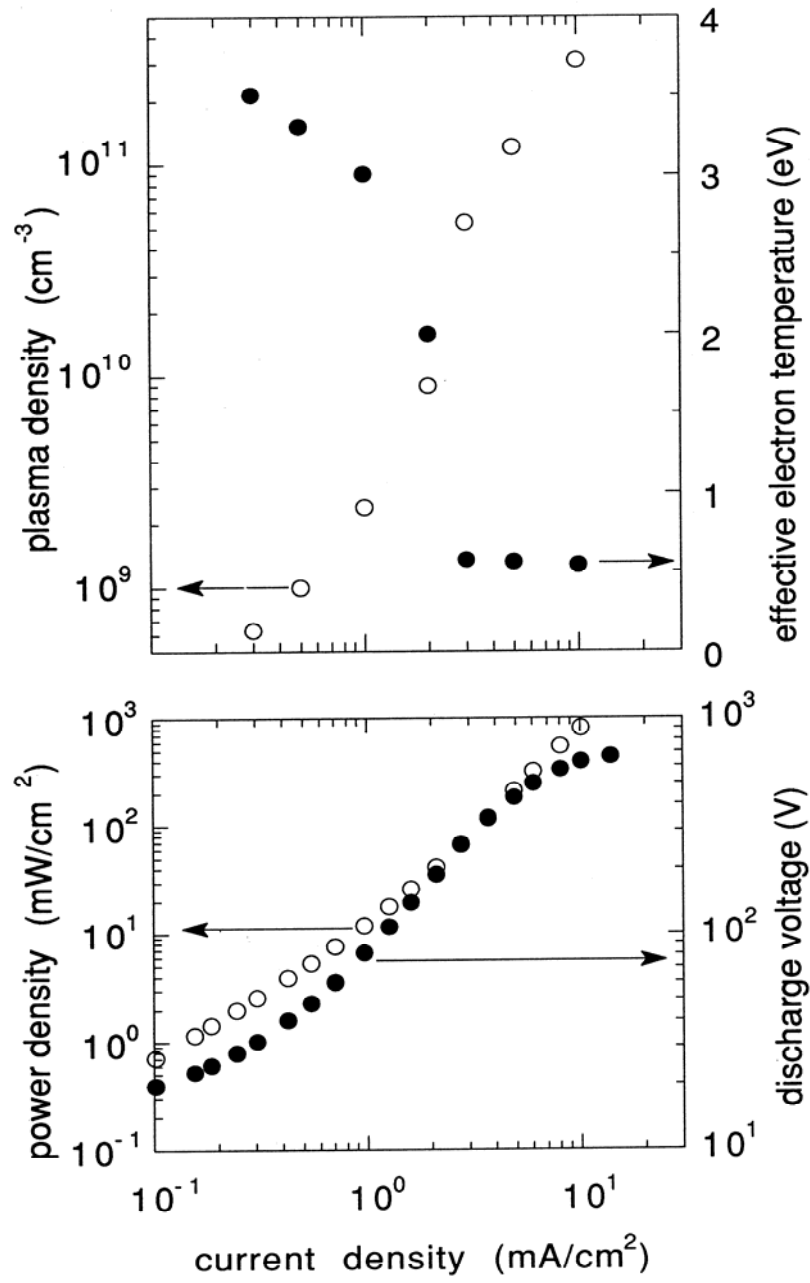


Fig. 7

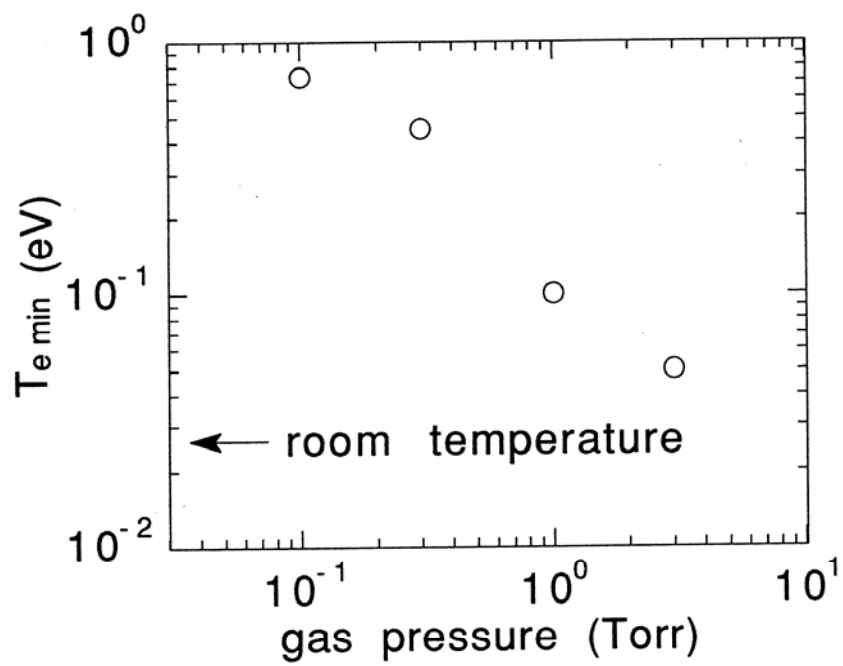


Fig. 8

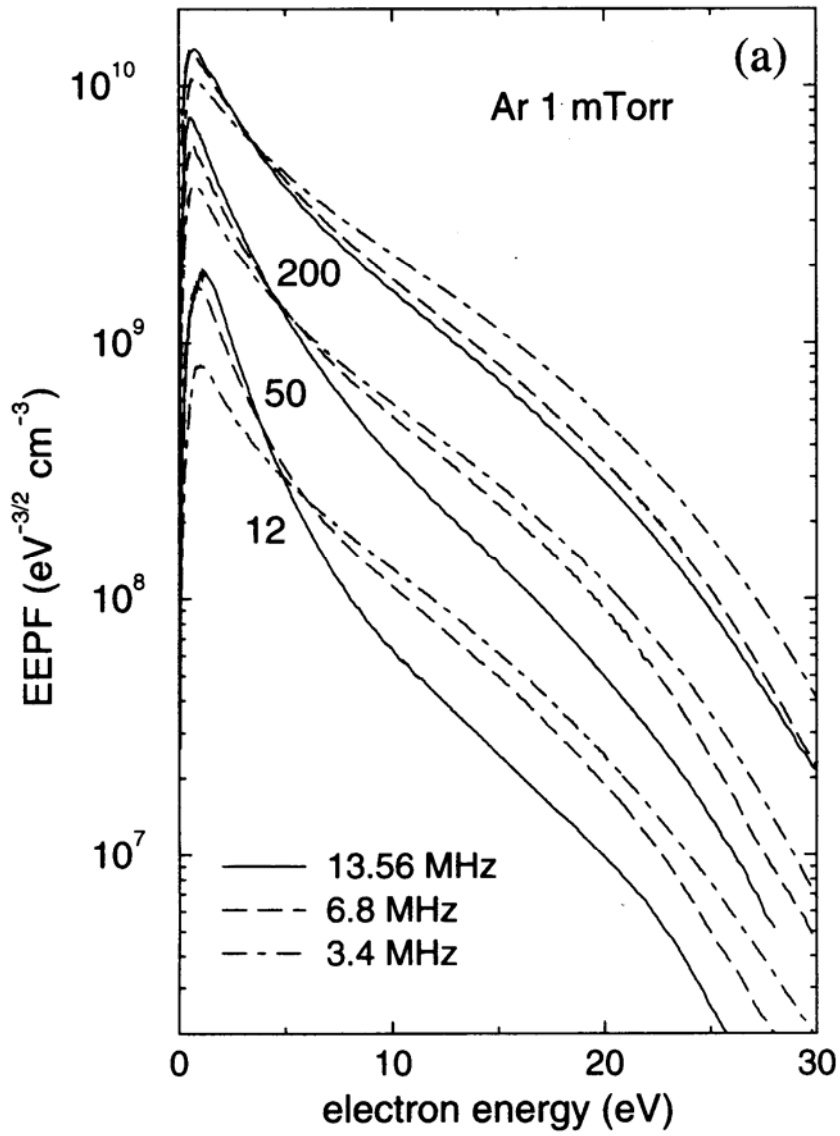


Fig. 9

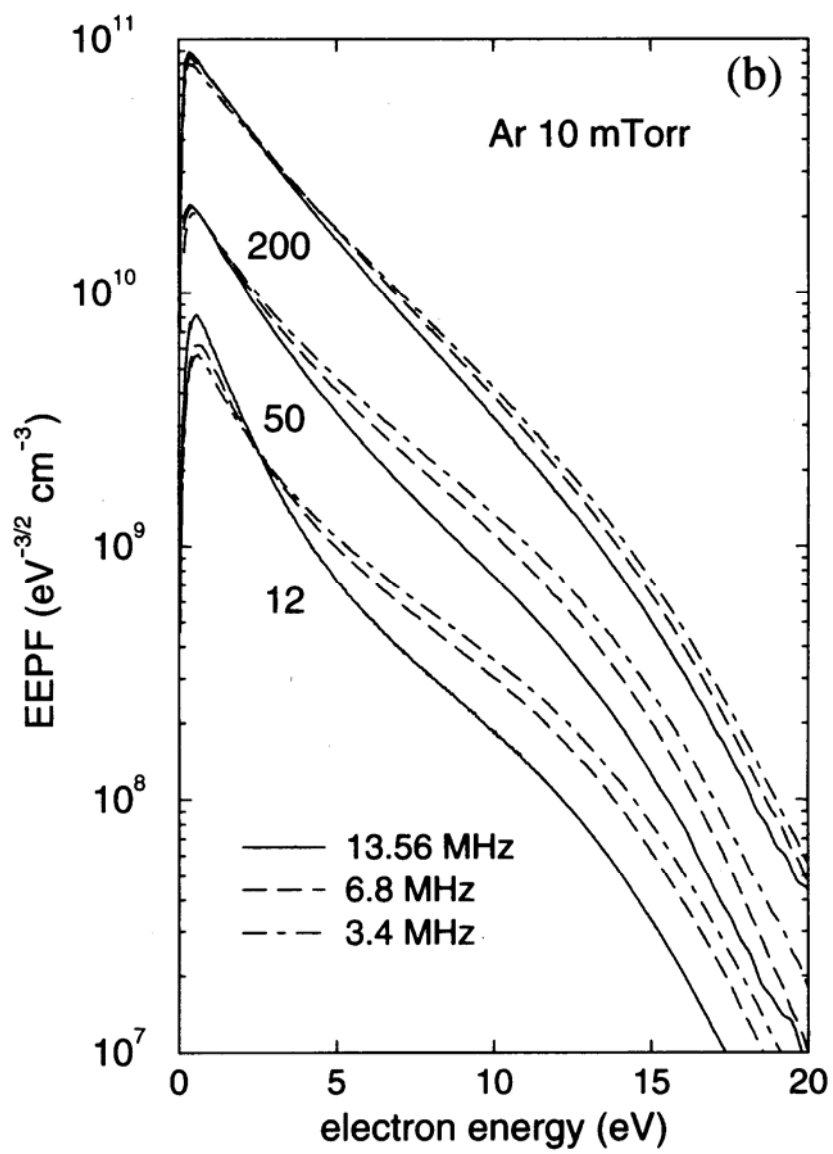


Fig. 10

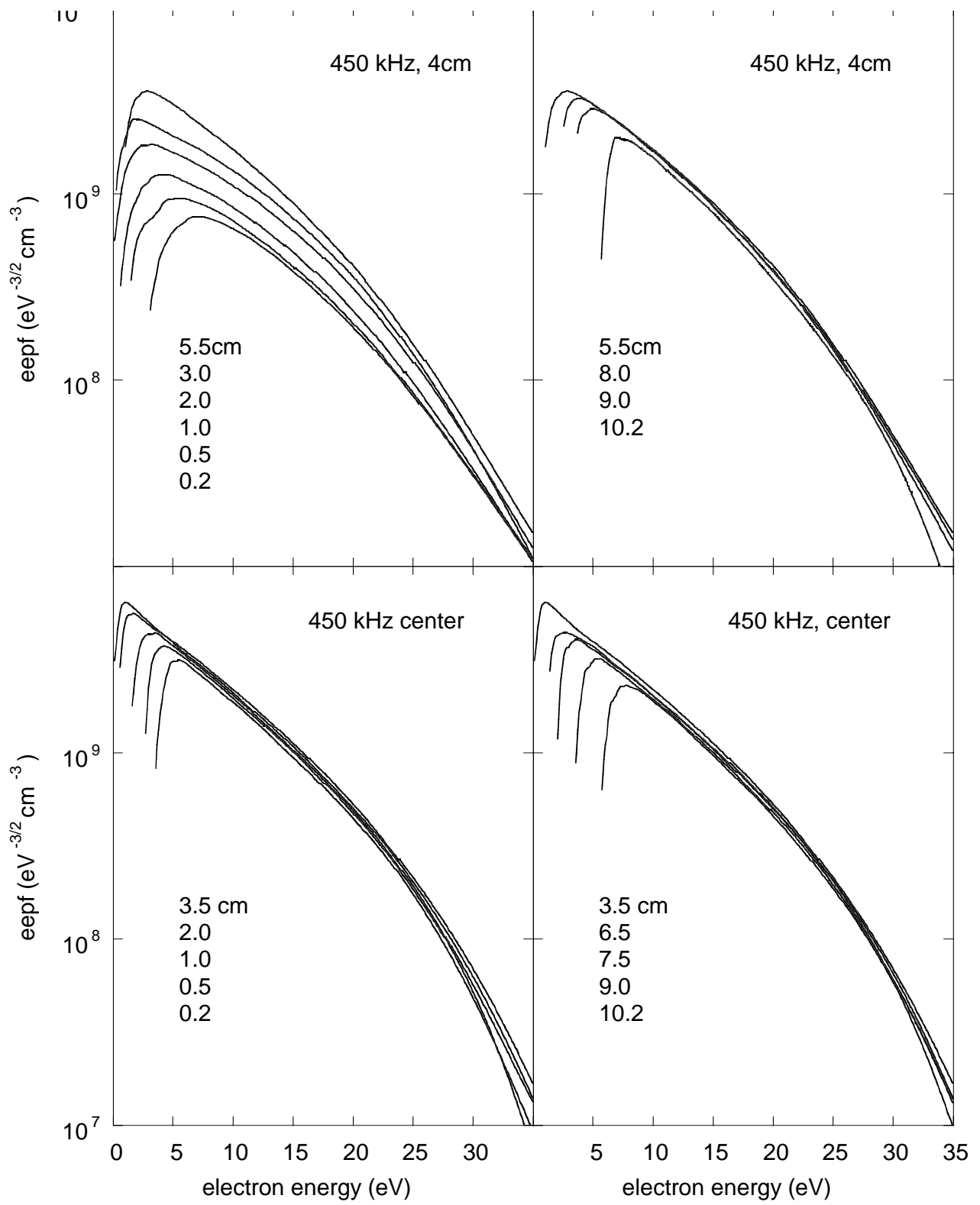


Fig. 11

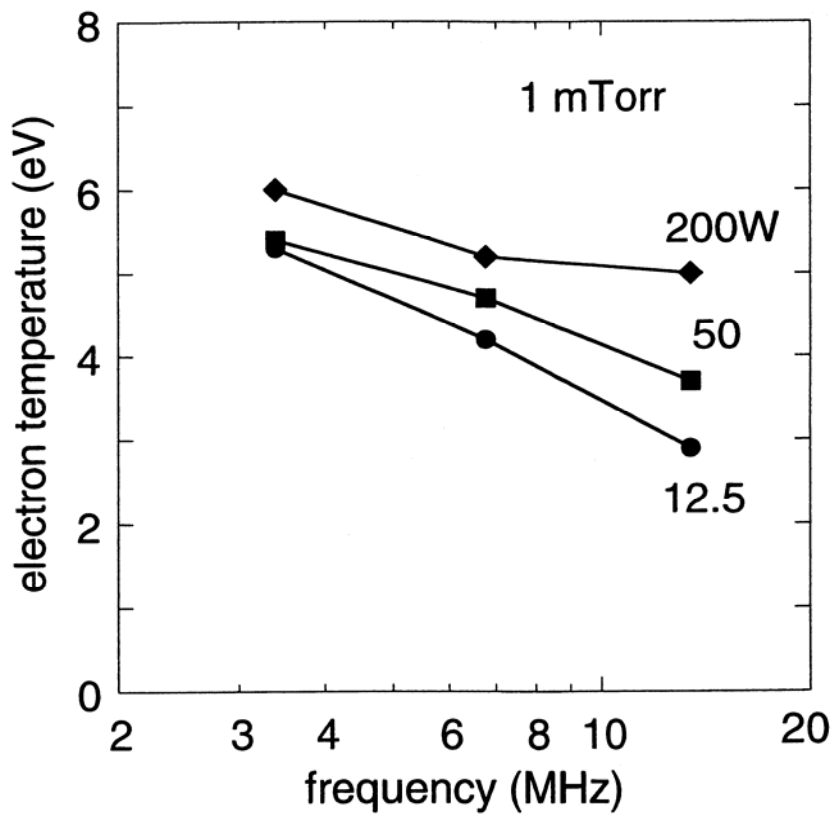


Fig. 12

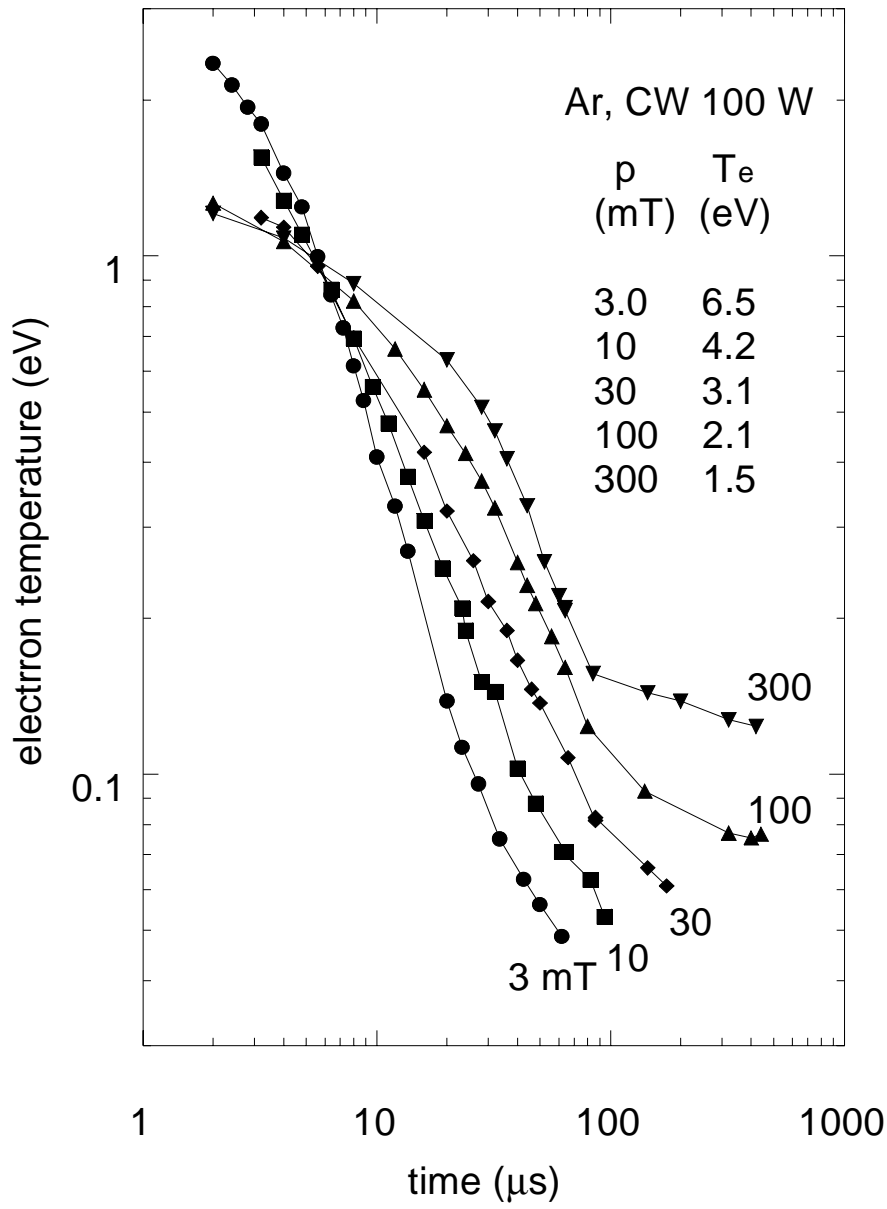


Fig. 13

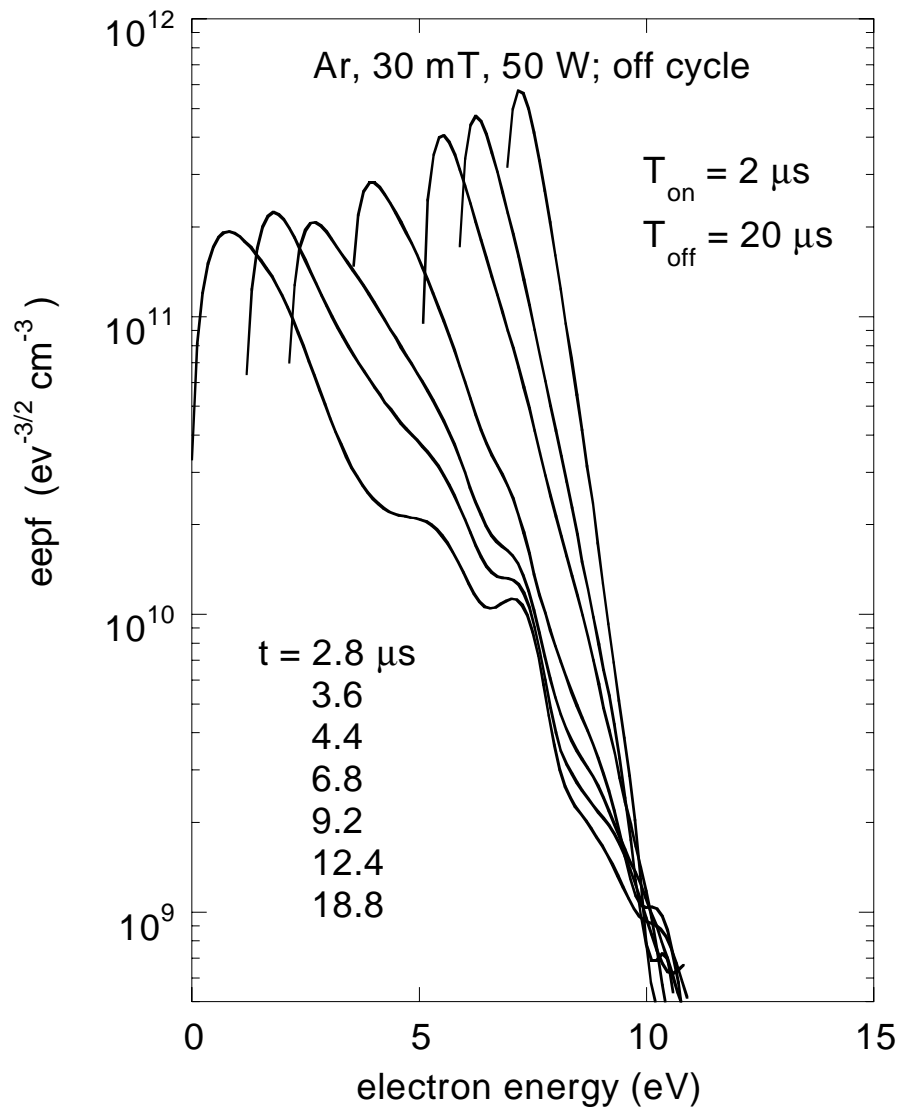


Fig. 14

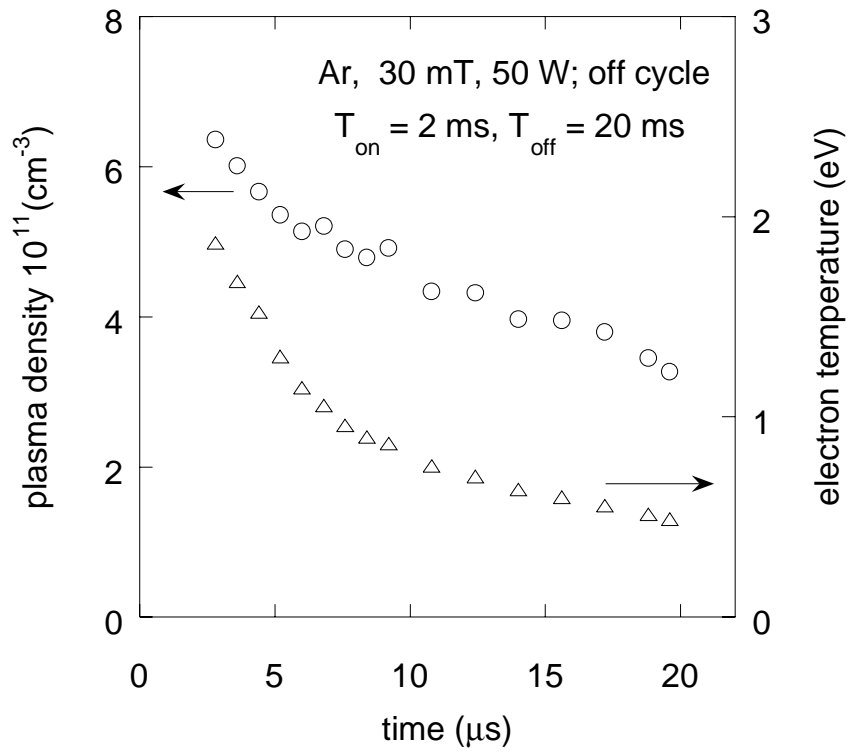


Fig. 15